Numerical simulation of gravity current descending a slope into a linearly stratified environment

Numerical simulation of gravity current descending a slope into a linearly stratified environment

Yakun Guo[1]; Zhiyong Zhang[2]; and Bing Shi[3]

Abstract: The accurate prediction of the dilution and motion of the produced denser water (e.g. discharge of concentrated brine generated during solution mining and desalination) is of importance for environmental protection. Boundary conditions and ambient stratification can significantly affect the dilution and motion of gravity currents. In this study, a multiphase model is applied to simulate the gravity current descending a slope into a linearly stratified ambient. The k-ω turbulence model is used to better simulate the near bed motion. The mathematical model, initial and boundary conditions and the details of the numerical scheme are described. The time-dependent evolution of the gravity current, the flow thickness and the velocity and density field are simulated for a range of flow parameters. Simulations show that the Kelvin–Helmholtz billows are generated at the top of trailing fluid by the interfacial velocity shear. The K-H type instability becomes weaker with the slope distance from the source due to the decrease of the interfacial velocity shear along slope. The ambient stratification restricts and decreases the current head velocity as it descends slope, which differs from the situation in homogenous ambient while the head velocity remains an approximately steady state.

[1]Reader, School of Engineering, University of Aberdeen, Aberdeen, AB24 3UE, UK. (corresponding author). Email: y.guo@abdn.ac.uk.

[2]PhD student, College of Engineering, Ocean University of China, Qingdao 266100, China; School of Engineering, University of Aberdeen, Aberdeen, AB24 3UE, UK. Email: zhiyongzhang@abdn.ac.uk. Present address: Postdoctoral Research Associate, Zhejiang Institute of Hydraulics and Estuary, Hangzhou, 310020, China.

[3]Professor, College of Engineering, Ocean University of China, Qingdao 266100, China. Email: sediment@ouc.edu.cn.

Motion of the descending flow into the stratified ambient has two stages: initial acceleration and deceleration at later stage based on the balance of inertial, buoyancy and friction forces. When the descending current approaches the initial neutral position at later stage, it separates from the slope and spreads horizontally into environment. The simulated results, such as vertical velocity and density profiles and front positions, agree well with the measurements, indicating that the mathematical model can be successfully applied to simulate the effect of the boundary condition and ambient stratification on the dilution and propagation of gravity currents.

Keywords: Gravity current; numerical models; simulation; stratification

Introduction

Gravity currents are flows driven by density gradient and are frequently encountered in both natural and man-made environments. Typical examples are saltwater intrusion in estuaries; oil spillage in the oceans and brine discharges from desalination or solution mining facilities. The saltwater wedge intrusion in estuaries occurs on non-uniform slopes and often influences the overall water quality and environment of estuaries while the discharge of denser water from desalination plants may greatly affect the environment and ecology of the ambient receiving water body. Due to the practical importance of gravity currents and their relevance and theoretical significance for a variety of flow phenomena, many studies have been conducted over the last few decades. Extensive studies have been conducted to investigate the simple gravity current scenario, i.e. flow moving along a horizontal surface into a homogenous fluid

(e.g., Simpson 1982, 1997) or stratified ambient receiving fluid (e.g., Holyer and Huppert 1980; Guo *et al*. 2000; Ungarish and Huppert 2002; Baines 2001, 2005; Maxworthy *et al*. 2002; Birman *et al.* 2007; Munroe *et al*. 2009). For most real situations (e.g., estuaries), however, the bottom solid boundary is not horizontal, and the flow feature of gravity current descending a slope can be very different from that over a horizontal surface. Such flow characteristics of the current descending a slope have recently received increasing studies, primarily using laboratory experiments.

Ellison and Turner (1959) investigated the gravity currents descending a slope into a tank using laboratory experiments. Based on the analysis of their experimental data, they derived a dynamic model for investigating the bulk proprieties of the flow. They found that the mean fluid velocity was only dependent on the local bulk Richardson number, *R*i and had no relation with the downslope distance. Britter and Linden (1980) obtained slightly different results for small slope though their finding for larger slope was similar to that of Ellison and Turner (1959). In their laboratory experiments, Britter and Linden (1980) found that for the small slopes (θ<0.5^o), the head of the gravity current decelerated with distance from the source while for larger slope, a steady head velocity was generated as the buoyancy force was sufficiently large to overcome frictional effects. Using internal hydraulic theory (Armi 1986), Lawrence (1993) investigated the flow regimes of two layer flow over a fixed obstacle using laboratory experiments. Such theory, however, cannot simulate the mixing at the interface of two fluids (Zhu and Lawrence 1998; 2000). The internal hydraulic theory was extended by

Zhu and Lawrence (1998; 2000) to examine the effects of non-hydrostatic and friction on exchange flow. They found that when the friction and non-hydrostatic effect were considered, more accurate prediction of interfacial mixing in the exchange flow was achieved. The method, however, requires information of the friction factor at the interface which may be difficult to obtain. Similar method was applied by Cuthbertson *et al.* (2004, 2006) who studied the buoyancy-driven exchange flow over a steadily descending barrier using the laboratory experiments. Maxworthy and Nokes (2007) and Maxworthy (2010) conducted laboratory experiments to investigate the propagation of gravity currents descending a slope. The current was generated by releasing a fixed volume of heavy fluid in a lock located at the top of the slope. They observed two flow stages: initial acceleration stage and deceleration stage. Dai (2013) conducted similar laboratory experiments and found that the flow patterns for gravity current descending a slope qualitatively differed from those moving along a horizontal bottom. In above studies, the ambient fluid was homogenous. Mitsudera and Baines (1992) firstly studied the gravity current descending a slope into a continuously stratified environment using laboratory experiments. This work was extended by Baines (2001; 2005) to investigate in details the effect of slope and ambient stratification on the flow features. From the experiments, Baines found that two flow regimes, gravity-current-like and plume-like which depended on the balance of buoyancy and drag, were formed as the flow descended the slope into a stratified ambient. A model was developed to calculate the mixing of gravity current with ambient fluid. The effect of ambient two-layer stratification on the motion of gravity currents was examined by Monaghan *et al.* (1999)

using laboratory experiments. They found that as the current gravity approached the sharp density interface; it was split into two parts: one propagating along density interface, another along the tank bottom.

With the development of computational science, mathematical models and numerical methods, which have advantages of scaling, less expense, adaptability, nonintrusion and transportability (Falconer 1992; Guo *et al.* 2007), have provided an alternative approach to simulate the motion of the gravity currents in past decades (Özgökmen *et al.* 2006). Bournet *et al.* (1999) applied the $k-\varepsilon$ model to simulate the gravity currents plunging into reservoirs. $k-\varepsilon$ model was also applied by Choi and Gracia (2002) to investigate the two dimensional (2D) denser underflow descending a slope into a homogenous environment. Zhang *et al.* (2008) applied the multiphase model to simulate the flushing of trapped salt water from a bar–blocked estuary. Birman *et al.* (2007) evaluated the effect of the slope on the front velocity by solving the two-dimensional NS equations in a homogeneous ambient. They showed that quasi-steady front velocity of the flow reached the maximum near the slope angle of 40 degree. Firoozabadi *et al.* (2009) simulated the 3D motion of denser underflows in a straight channel by using the lower Reynolds number $k-\varepsilon$ model. Their simulation was in good agreement with their experiments. Ooi *et al.* (2009) conducted 2D large eddy simulation (LES) to model the motion of the gravity current generated by lock exchange. They found that their 2D LES model can capture most important flow features such as the front evolution and the formation of coherent billow structures at

the flow head. LES was also applied by Mahdinia *et al.* (2012) to investigate the lock exchange flow in a curved channel. Dai *et al*. (2012) and Dai (2013) performed 3D direct numerical simulation (DNS) for gravity currents generated from instantaneous sources descending a slope into a homogeneous environment. They found that the flow structure for lower slope angle was slightly different from that of steeper slope. Härtel *et. al.* (2000) performed 3D (for the lower Reynolds number up to 750) and 2D (for the Reynolds number up to 30,000) DNS for lock exchange flow to investigate the propagation of gravity current fronts. Their simulation showed that the 2D model was able to capture essential flow features of the current front. More research work on the motion of gravity currents and turbidity currents can be found in Simpson (1982, 1997) and Meiburg and Kneller (2010).

Though these studies demonstrated some flow characteristics of gravity currents moving in various boundary conditions, none of these numerical studies considered the combined effect of ambient stratification and bottom slope on the movement of gravity currents. Therefore, references to the numerical modelling studies for gravity currents descending a slope into a stratified environment are still lacking. In fact, experiments of Baines (2001, 2005) demonstrated that the stratification in receiving environment can significantly influenced the motion of gravity current. Such effect of the combination of ambient stratification and bed slope on the motion of gravity current was examined by Özgökmen *et al.* (2006) who conducted the numerical simulation to investigate the transport of large scale gravity currents in oceans. They found that when the gravity

currents separated from the slope bed, the transport of the flow only depended on the strength of the ambient stratification. Their study only focused on the bulk properties of the motion of the large scale gravity currents and didn't investigate the details of the flow structure. Such information is important for predicting the dilution and motion of the produced denser water (e.g. from desalination or mining solution) discharging into the receiving water bodies, which is the major concern from the point of view of environment protection. This is the motivation of this study in which a two-dimensional multiphase model is employed to simulate the flow structures and density distribution within the gravity current as it descends a slope into a linearly stratified environment. The evolution of the gravity current and front motion, the flow thickness, the vertical density distribution and velocity profiles within the flow are simulated for a range of flow conditions. Simulated results are in good agreement with the laboratory measurements of Mitsudera and Baines (1992) and Baines (2001; 2005).

Multiphase model

Governing equations

As different phases (inflow source water, surface salt water and the bottom salt water) share the same velocity and pressure field, the governing equations are a single set of momentum and continuity equations in conservative form (Ferziger and Perić 2002):

$$\frac{\partial}{\partial t}(\alpha_q \rho_q) + \nabla \cdot (\alpha_q \rho_q \vec{v}_q) = 0 \tag{1}$$

$$\frac{\partial}{\partial t}(\alpha_q \rho_q \vec{v}_q) + \nabla \cdot (\alpha_q \rho_q \vec{v}_q \vec{v}_q) = -\alpha_q \nabla P + \nabla \cdot \bar{\bar{\tau}}_q + \alpha_q \rho_q \vec{g} + \sum_{p=1}^{3} K_{pq}(\vec{v}_p - \vec{v}_q) \tag{2}$$

$$\overline{\overline{\tau}}_q = \alpha_q \mu_q (\nabla \vec{v}_q + \nabla \vec{v}_q^T) + \alpha_q (\lambda_q - \frac{2}{3}\mu_q) \nabla \cdot \vec{v}_q \overline{\overline{I}} \quad (3)$$

where p and q = the phase constituent; α_q = volume fraction of phase q (the volume fractions for all phases sum to one); ρ_q=the density of phase q; $\vec{v}$ =the velocity vector; $\overline{\overline{\tau}}_q$ =the stress-strain tensor of phase q; μ_q, λ_q = the coefficients of shear and bulk viscosity of phase q, respectively; $\overline{\overline{I}}$ = unit tensor; P =the pressure shared by phases; $\vec{g}$ =the gravity acceleration; and K_{pq} = the momentum exchange coefficient between phases.

Turbulence model

In the simulation of gravity current, the near bed flow features have a significant effect on the spreading and propagation of the gravity current. To accurately model this near bed flow feature, a low Reynolds number k-ω model, which better models the near wall flow, is applied. The governing equations are as following (Wilcox 2006; 2008):

$$\frac{\partial}{\partial t}(\rho k) + \frac{\partial}{\partial x_i}(\rho k u_i) = \frac{\partial}{\partial x_j}[(\mu + \frac{\mu_t}{\sigma_k})\frac{\partial k}{\partial x_j}) + G_k - Y_k \quad (4)$$

$$\frac{\partial}{\partial t}(\rho \omega) + \frac{\partial}{\partial x_i}(\rho \omega u_i) = \frac{\partial}{\partial x_j}[(\mu + \frac{\mu_t}{\sigma_\omega})\frac{\partial \omega}{\partial x_j}) + G_\omega - Y_\omega \quad (5)$$

$$\rho = \sum_{p=1}^{3} \alpha_p \rho_p \quad (6)$$

$$u_i = \frac{\sum_{p=1}^{3} \alpha_p \rho_p \vec{v}_p(i)}{\sum_{p=1}^{3} \alpha_p \rho_p} \quad (7)$$

where ρ =the mixture density of all phases; k = the turbulent kinetic energy; μ =the dynamic viscosity of water; t =the time; u_i =the component of velocity in the

x_i-direction; ω =the specific dissipation rate; μ_t =the turbulent (or eddy) viscosity; σ_k, σ_ω =the turbulent Prandtl number for k and ω, respectively; G_k =the generation of k induced by the mean velocity gradients; G_ω =the generation of ω caused by the mean velocity gradients; Y_k =the dissipation of k due to turbulence; and Y_ω =the dissipation of ω due to turbulence.

The term of turbulent kinetic energy produced by the mean velocity gradients and turbulent viscosity can be determined by (Wilcox 2006; 2008):

$$G_k = \mu_t \left(\frac{\partial u_i}{\partial x_j} + \frac{\partial u_j}{\partial x_i}\right)\frac{\partial u_i}{\partial x_j} \tag{8}$$

$$\mu_t = \frac{0.144\mu\omega + \rho k}{6\mu\omega + \rho k}\frac{\rho k}{\omega} \tag{9}$$

$$\omega = \frac{\varepsilon}{C_\mu k} \tag{10}$$

where ε = dissipation rate of k. The values of the constants are (Rodi 1993; Wilcox 2006): σ_k =2.0; C_μ=0.09; and σ_ω =2.0.

Numerical scheme

The governing equations are solved by finite volume method (FVM). The discretized form of continuity equation can be expressed as (Versteeg and Malalasekera 1995):

$$A_1^c \Omega^c = \sum_{nb} A_1^{nb} \Omega^{nb} \tag{11a}$$

$$\Omega = (\alpha_1, \alpha_2, \alpha_3)^T \tag{11b}$$

A_1^c, A_1^{nb}= the coefficients matrices that contain the influence from transient and convection terms where superscript c refers to cell center and superscript nb refers to

cell neighbors, respectively; Ω = vector of phases. Applying Eq.(11) and $\sum_{p=1}^{3}\alpha_p = 1$ yields the volume fractions of phases.

The transient, convection, pressure, diffusion, gravity and momentum exchange terms in momentum equation can be discretized as (Cokljat *et al.* 2006)

$$(\overline{A}^c - \overline{R}^c)\vec{U}_q^{\,c,*}(i) = \sum_{nb}\overline{A}^{nb}\vec{U}_q^{\,nb,*}(i) - \Omega^c\frac{\partial P^*}{\partial x_i} + \overline{B}_q^{\,c,n} \tag{12a}$$

$$\vec{U}_q^{\,*}(i) = (\vec{v}_1^{\,*}(i), \vec{v}_2^{\,*}(i), \vec{v}_3^{\,*}(i))^T \tag{12b}$$

where $\overline{A}^c$, $\overline{A}^{nb}$ = the coefficients matrices that contain the influence from transient, convection and diffusion terms (superscript *c* and *nb* have the same meaning as in Eq.(11); $\overline{R}^c$ = the matrices representing the momentum exchange term; $\overline{B}^c$ = gravity term; $\vec{U}_q$ = phase velocities vector. Superscript * represents the current iteration and *n* refers to the previous iteration.

The turbulence equations can be discretized similarly to those used for continuity equation. The pressure-velocity coupling is achieved with the use of the phased coupled SIMPLE (PC-SIMPLE) (Vasquez and Ivanov 2000), an extension of the SIMPLE algorithm (Spalding 1980) to multiphase flows. The QUICK scheme is applied for spatial discretization of governing equations, while the second order implicit scheme is used for temporal discretization (Ferziger and Perić 2002). The velocities are solved and coupled by phases in a segregated fashion. Fluxes are reconstructed at the faces of the control volume and then a pressure correction equation is built based on total

212 continuity. The coefficients of the pressure correction equations come from the coupled
213 per phase momentum equations (Vasquez and Ivanov 2000). Body-fitted non-uniform
214 meshes with arbitrarily spatially dependent size were used in order to accurately fit the
215 slope bed in the computational domain. This allows for locally refining the concerned
216 regions (e.g. near bed region) with small meshes and has the advantage of flexibly
217 assigning meshes in the computational domain (Guo *et al*. 2008, 2012; Jing *et al*. 2009).
218 Sensitivity analysis of mesh size was carried out by adapting and refining the meshes
219 until no noticeable changes in the solution was achieved (Guo 2014). Several mesh
220 sizes have been investigated and compared in terms of the simulation accuracy,
221 convergence and computational time to determine the final meshes (see section: Results
222 and discussion). The final meshes having 266000 elements were used in the simulation
223 with the minimum and maximum grid size in *x*-direction being 0.0015m and 0.012m,
224 and 0.00015m and 0.0006m in *z*-direction, respectively. The maximum residual for
225 convergence was 10^{-5} with a constant time step being 10^{-4} s.
226
227 ***Initial and boundary conditions***
228 The computational domain is shown in Figure 1. At the inlet boundary, velocity profile
229 is specified using the experimental data. Turbulent kinetic energy *k* and specific
230 dissipation rate ω are set as following (Ferziger and Perić 2002):

231 $$u = u_0;\ w=0 \tag{13}$$

232 $$k_{in} = 10^{-4} u_0^{\ 2} \tag{14}$$

233 $$\omega_{in} = 10 k_{in}^{0.5} / (c_\mu d_0) \tag{15}$$

where u_0 and w = the initial mean velocity in x- and z-direction at the inlet, respectively (see Fig. 1); d_0 = the initial thickness of the inflow at the inlet. The pressure outlet boundary condition is specified at the outlet in which a static pressure at the outlet boundary is realized. At the free water surface, the atmospheric pressure is applied. The non-slip boundary condition is applied on all solid walls. The standard wall function law is used to estimate the velocity parallel to the slope bed at the first cell (Launder and Spalding 1974).

In order to observe the evolution of the gravity current, the inflow source water, the surface salt water and the bottom salt water in the tank are treated as three single miscible phases. The densities of the surface and bottom salt water phases in the tank are defined to generate the prescribed ambient stratification, which can be expressed as:

$$\rho = \rho_2 - (\rho_2 - \rho_1) z / Z_0 \tag{16}$$

where ρ_1 and ρ_2 = the water density at the surface and the bottom of the tank, respectively; Z_0 = water depth in the tank (see Figure 1).

Procedure of solution

The procedure of the solution for governing equations is:

1. Specify initial and boundary conditions
2. Solve the phase continuity equations
3. Construct the momentum equation matrix
4. Predict the pressure field.

5. Solve the momentum equation and obtain the velocity field
6. Correct the pressure and update the velocity field
7. Solve the transport equations for the turbulence quantities
8. Repeat steps 2 to 7 until the prescribed computational accuracy is achieved
9. Using the calculated variables from the current time step as initial conditions and repeat steps 2 to 8 to calculate the variables of next time step until $t=t_{max}$.

Experiments

Laboratory experiments carried out by Mitsudera and Baines (1992) and Baines (2001; 2005) are used to validate the model. Though the details of the experiments can be found in Mitsudera and Baines (1992) and Baines (2001; 2005); a brief description of the experiments is presented for completeness and convenience. Figure 1 is a modified sketch of the laboratory experiment under investigation. The experiments were carried out in a rectangular tank of 38 cm wide, 299 cm long and 80 cm high. A thin vertical partition was inserted to extend the effective working length. The tank was initially filled with continuously/linearly stratified fluid using the two-tank technique (Davies *et al.* 1995). The ambient stratification was measured by a conductivity probe and was used for calculating the control parameters (see below). A horizontal platform of 40 cm long (not shown in Fig. 1) was inserted from one end of tank and was connected with the sloping bottom which extended into the main portion of tank. On the platform, a water-tight removable sluice gate was installed at a distance of 31 cm from the tank end. Denser water (dyed to facilitate the observations) was filled behind this removable gate.

The gravity current was generated and descended the slope into the initially quiescent stratified ambient when the gate was suddenly lifted. Constant denser flow rate was maintained and monitored by a flow meter in the inflow hose throughout the experiment. For more details of experiments, readers are referred to Baines (2001, 2005).

To facilitate the description of the flow, the following parameters are defined (Baines, 2001; 2005):

$$N^2 = \frac{g_0^{'}}{D} \tag{17}$$

$$g_0^{'} = g\frac{\rho_{in} - \rho_{top}}{\overline{\rho}} \tag{18}$$

$$B_0 = \frac{Q_0 N^3}{g_0^{'2}} \tag{19}$$

$$Re = \frac{Q_0}{\nu} = \frac{u_0 d_0}{\nu} \tag{20}$$

where ρ_{top} = the density of ambient water in tank at the top of slope; ρ_{in} = the density of inflow which is equal to the water density in the tank at the vertical depth D from the top of the slope (see Figure 1); $\overline{\rho}$ = the mean density of ρ_{top} and ρ_{in}; ν = the kinematic viscosity of water; N = the buoyancy frequency of the initially undisturbed density stratification in the tank; $g_0^{'}$ = the reduced gravity acceleration; Q_0 = the initial volumetric flow rate per unit slot width; Re = the Reynolds number and B_0 the buoyancy number of the flow. From the definition, B_0=0 corresponds to a homogeneous environment and B_0 increases with the increase of the strength of the ambient stratification for the same initial volumetric flow rate.

The range of the experimental parameters was: volumetric flow rate Q_0=4×10^{-5}-1.121×10^{-3} m^2/s; inlet height d_0=0.01m; inlet velocity u_0=0.004-0.1121 m/s; the slope angle θ=6°; D=0.10 – 0.206 m; the reduced gravity acceleration of inlet salt water g'_0=5.75-31.63 cm/s^2; the water depth Z_0=0.23m and the vertical distance between the top of slope and the bottom of tank is 0.2 m. These values yield the buoyancy number B_0=0.0014-0.0734 and the inflow Reynolds number Re=40-1121. The numerical simulation runs cover the range of these parameters.

Results and discussion

Mesh sensitivity analysis

To investigate the effect of mesh sizes on the computational accuracy and time as well as the convergence, three meshes of coarse (106400), medium (266000) and fine (500000) were used in the simulation. The corresponding minimum and maximum mesh sizes in x- and z-directions are: 0.002m and 0.015m (x-direction), 0.000375m and 0.0008m (z-direction); 0.0015m and 0.012m (x-direction), 0.00015m and 0.0006m (z-direction); and 0.0005 m and 0.008m (x-direction), and 0.000075m and 0.0008m (z-direction); respectively. The simulations were performed on a PC workstation: HP Z650 with 6 cores, CPU 2.30GHZ, 2 processors and 48GB memory. For all mesh sizes simulated, a convergent solution was always obtained. The computational accuracy and time, however, was different. Fig. 2 is the comparison of the simulated velocity profiles at x=0.7m using three meshes with the experimental measurements (Mitsudera and Baines 1992) for the flow with initial B_0=0.022 and Re=290. It is seen that the

computational results using medium and fine meshes are similar and agree well with the experimental results, while relatively large deviation exists between the simulated results using coarse meshes and measurements. The computational times for 100s are 10.2 hours (coarse), 36.8 hours (medium) and 126.5 hours (fine) respectively. Simulations performed for different flow parameters obtain the similar results. Considering the computational accuracy and time, the final mesh used is 266000 (medium).

Evolution of the gravity current and the front motion

To facilitate the analysis and compare with the experimental measurements, an along (s) and normal to the slope (r) coordinate system s-r is used (see Figure 1. Note that the simulation was performed in x-z coordinate system). In this coordinate system, u_s refers to the downslope component of velocity. For a homogeneous environment, it is well known that the typical motion of the gravity current descending a slope has a raised head in the front, followed by a shallower steady current. This continues to flow to the end of slope provided that the buoyancy is sufficiently large. However, for the cases of the stratified environment, the situation is different. Figure 3 is a time series plot of the simulated evolution of a gravity current descending a slope into a linearly stratified environment in which the initial density of the current at the inlet is smaller than the density of the ambient fluid near the tank bottom. Once the denser water intrudes the ambient fluid, a front at the leading edge is quickly formed and flows down slope (see Fig. 3a). A velocity shear layer is established at the interface between the flowing

current and initially quiescent ambient fluid. This shear velocity generates mixing at the interface and entrains surrounding lighter fluid into the flow. As such, the flow, particularly the front and leading part of the current, is diluted and grows as it moves along the slope (see Fig. 3b, c, d). It is seen from Fig. 3c and d that the Kelvin–Helmholtz billows (Baines 2001) are formed at the top of the trailing fluid – a flow pattern also found in large scale simulation (Özgökmen *et al.* 2006). This means that the local gradient Richardson number across the interface Ri_g (=-{$g(\partial\rho/\partial z)/[\rho_r(\partial u/\partial z)^2]$}, ρ_r=reference density, Moore and Long 1971) is sufficiently low for the Kelvin-Helmholtz type billows to appear in the region of the trailing. As the flow moves down slope, the velocity and density, thus the buoyancy and inertial, of the leading front of flow decreases. This process continues until the inertia and buoyancy of the flow front cannot overcome the bottom friction and ambient stratification. As a result, the nose of the current thickens and separates from the bottom of slope (Figure 3c-d) and spreads horizontally into the environment before it reaches the end of the slope. The ambient fluid below the position at which the flow separates from the slope (separation point) is undisturbed. The position of the separation point partly depends on the degree of the interfacial shear generated mixing and entrainment of the flow with ambient fluid. This shear generated mixing and entrainment at the interface of flow and ambient fluid is determined by the flow condition (B_0=0.02 and *Re*), the bed slope and ambient stratification. Simulations have been performed for a range of parameters, demonstrating that this position is usually not much lower than the neutral position where the density of ambient fluid is equal to the initial density of the flow at the inlet

(e.g. the vertical extension of the flow from the top of the slope is usually not much larger than the depth D).This means that no significant overshooting of the downflow over its initial neutral level occurs for the range of parameters investigated here though overshooting was usually observed in the experiments for high slope degree ($>30^0$) in which higher inertia of the downflow was expected.

Britter and Linden (1980) found that the head velocity kept a nearly constant value when slope angle $\theta \geq 0.5^0$ in homogenous environment. This means that a linear relationship between the time and the slope distance that the head of the flow travels exists. However, this is not the case when ambient fluid is stratified. Figure 4 plots the dimensionless position of current head against the travelling time for various flow conditions for the slope angle of 6 degree. Experimental results of Mitsudera and Baines (1992) for B_0=0.022 and Re=290 are also plotted in Fig. 4 for comparison where $s^*=s/D$. The slope distance corresponding to the buoyancy depth D (the initial neutral depth) is $D/sin(6°)=9.567D$. It is seen from Fig. 4 that at early stage, the velocity of the current head is roughly constant for all flow conditions simulated. As the buoyancy number and the flow Reynolds number increases (e.g. larger buoyancy and initial and more turbulent flow); the front of the current travels faster downslope, particularly at larger times. As time goes, the current head decelerates. This flow deceleration is caused by the decrease of the flow buoyancy and inertial along the slope due to (i) the increase of the density of the ambient fluid along the slope and (ii) the decrease of the flow velocity and density caused by the interfacial velocity shear generated mixing and

entrainment of flow fluid with ambient lighter fluid. The slowed current separates from the slope and spreads into environment before it reaches the neutral level for B_0=0.0072 and Re=267. For larger buoyancy and more turbulent flow (e.g. B_0=0.022, Re=290; and B_0=0.0734, Re=839), however, the current continues to flow down slope and slightly overshoots the neutral level due to the flow inertia. The simulation demonstrates that the distance of such overshooting increases with the increase of B_0 and Re (see Fig.4). In general, the numerically simulated front position reasonably agrees with the measured ones, particularly at the early stage. At larger times, the simulated distance that the current head travels along the slope is slightly smaller than that of the experimental measurements, indicating that the numerical model may slightly overestimate the mixing which results in a slower motion of the flow.

Vertical density profile

The vertical density profiles within the gravity current are simulated for a range of flow parameters, demonstrating similar interfacial shear generated vertical density distribution within the current. Figure 5 is a typical example of the vertical density profile (normal to the slope) at s=0.7 m for B_0=0.022 and Re=290 in which the depth denotes the normal distance from the slope bottom. It is seen that a sharp density jump takes place at about 0.01~0.015m from the slope bottom. This sharp density jump interface divides flow into two parts: the upper turbulent mixing layer and the bottom undisturbed/mixed or less disturbed/mixed current core whose density is almost the same as that of the current at the inlet. This density interface almost coincides with the

409 velocity shear interface (see Fig. 8 below) where the mixing and entrainment of flow
410 fluid with ambient fluid takes place. Such mixing and entrainment, thereby, generates a
411 layer of weak density stratification/gradient or almost homogenous immediately above
412 the interface (see Fig.5). Above this well mixed layer, there is little motion and the
413 ambient stratification is almost not disturbed. The comparison shows that in general,
414 the simulated density distribution agrees well with the experimental measurements of
415 Mitsudera and Baines (1992).
416
417 ***Thickness of the current***
418 Figure 3c and d shows that when the current approaches the initially neutral level, the
419 front of current thickens and separates from the slope bed and then propagates
420 horizontally into environment. At this stage, the thickness of the gravity current along
421 the slope does not change significantly with time though some obvious spatial variation
422 exists along the slope. Relatively small thickness at the inlet is found while a thicker
423 gravity current takes place near the separation point (see Figure 3c and d and Figure 6a,
424 b). This may be ascribed to the fact that the ambient fluid entrained into the flow
425 increases the volumetric flux along the slope while the downslope flow velocity
426 decreases with the slope distance away from the source (see Figure 4 and 8), resulting
427 in the increase of the thickness of the flow along the slope. Figure 6 also demonstrates
428 that the thickness of the gravity current has a relation with the buoyancy number B_0.
429 For relatively small B_0 (0.0072) and *Re* (267), the thickness of the current upstream of
430 the separation point is smaller; while the thickness is larger for relatively larger B_0

(0.0462) and *Re* (1121). To investigate the dependence of the current thickness on B_0, Figure 7 plots the spatially averaged dimensionless thickness of the current (normalized by the buoyancy depth *D*) versus B_0 in which the sharp density interface is used to determine the boundary of the current (see Figure 5). The experimental results of Baines' (2001) are included in Figure 7 for comparison. Though the data in Figure 7 is somewhat scattered, it is seen that in general, both the simulated and measured averaged thickness of the current increases with the increase of the flow buoyancy number B_0, which is consistent with Fig. 6. Figure 7 shows that the simulated spatially averaged thickness of the current reasonably compares with the laboratory measurements. For larger B_0, however, the simulated thickness of the current is larger than the measured ones, indicating that the numerical model overestimates the mixing, which is consistent with the result of Figure 4.

Velocity profile

The velocity field is simulated in the computational domain for a range of flow parameters and compared with the available experimental data. Figure 8 is an example to show the comparison of the simulated and measured (Mitsudera and Baines 1992) vertical velocity profiles at four cross sections for B_0=0.022, *Re*=290 and the initial current velocity of 0.029 m/s at the inlet. Figure 8 reveals that the similar velocity profiles are found at the different distance from the inlet. Velocity profiles at various positions demonstrate that the velocity increases sharply from zero on the slope bed where the no-slip condition is applied and reaches the maximum value at about 0.01m.

453 The flow velocity then decreases sharply and reaches the minimal value at about the
454 height of 0.015m near the inlet (s=0.1m, Figure 8a) and of 0.02m away from the inlet
455 (s=0.9m, Figure 8e). Comparing velocity profiles at different distance from the source
456 shown in Fig. 8 reveals that the flow velocity decreases with the distance from the
457 source while the current thickness increases along slope (see also Fig. 6) due to the
458 mixing and entrainment of the flow with lighter ambient fluid. The velocity shear layer
459 in Figure 8 roughly coincides with the density interface shown in Figure 5. Figure 8
460 also shows that negative velocity appears near the free surface in both the simulation
461 and experiments. This may be caused by the confined geometry used in the experiments
462 and simulation where a reflection from the end wall takes place to respond the intrusion
463 of the current when it is released into the tank. This negative velocity may not exist in
464 the real situation in which the environment is sufficiently large to avoid any reflection.
465 However, the negative velocity is very small and has little effect on the motion of the
466 flow. In general, the simulated velocity profiles are in good agreement with the
467 experimental measurements, particularly at the distance close to the inlet. Some
468 discrepancy between the simulations and measurements exists at the position away
469 from the inlet, e.g. s=0.7m and 0.9m. This discrepancy may be ascribed to the fact that
470 the present model is 2D which may not be able to capture the details of flow near the
471 neutral buoyancy level where stronger flow fluctuation takes place, indicating the 3D
472 flow features. To accurately simulate the details of the flow in this region, 3D
473 numerical model is required.
474

Numerical simulations are also performed for a range of flow parameters to evaluate and investigate their effects on the maximum flow velocity along the slope. Figure 9 compares the simulated and measured (Mitsudera and Baines 1992) relative maximum velocity (normalized by the initial flow velocity at the inlet) along the slope for various inflow Re and B_0. It is seen that when Re and B_0 are smaller (Re=267, B_0=0.0072; and Re=290, B_0=0.022), the maximum velocity has a sharp increase near the inlet and reaches the maximum value which is almost twice of the inlet flow velocity. This may be ascribed to the decrease of the flow thickness in the region near the inlet (see also Figure 6(a)) while the mass conservation makes the flow velocity increase. The maximum velocity then gradually decreases with the distance from the source due to the interfacial mixing and entrainment-induced decrease of buoyancy and the viscosity loss. For larger Re and B_0 (Re=839, B_0=0.0734; and Re=1121, B_0=0.0462), however, the situation is different. In these cases, the flow is more turbulent so that significant mixing and entrainment between flow and ambient fluid takes place immediately as the flow intrudes into the environment. As a result, the flow thickness increases with the distance from the source (see Figure 6(b)), leading to the decrease of the flow velocity. Figure 9 also demonstrates that the relative maximum velocity for smaller Re and B_0 is larger than that for larger Re and B_0 flow as the latter generates stronger mixing and entrainment along slope, thus slowing the current. In general, simulated relative maximum velocity favorably compares with the experimental measurements.

Conclusions

Gravity currents are ubiquitous in both natural and man-made environments (e.g. saltwater intrusion in estuaries; discharge of concentrated brine generated during solution mining and desalination). The accurate prediction of the spreading and motion is of importance from the point of view of protecting water quality in natural systems. As such, details of velocity field and density distribution within the current are essential. In this study, a multiphase model with k-ω turbulence model is applied to investigate the gravity current descending a slope into linearly stratified environment. Velocity and density fields are simulated for a wide range of flow parameters, including source denser flow rate and density, initial buoyancy frequency of the ambient fluid. The evolution of gravity current, head velocity, vertical velocity and density profiles are simulated and compared with the available experimental measurements. The simulations show that the flow characteristics can be described using a group of dimensionless numbers, namely the flow Reynolds number and buoyancy number defined by Baines (2001, 2005). Simulated results demonstrate that the ambient stratification has significant effect on the gravity current: (1) the current head velocity decreases along the slope in ambient stratification while in homogeneous environment, the head velocity maintains roughly a constant value for slope angle $\theta \geq 0.5^0$ (Britter and Linden 1980); (2) flow separation from the slope bed takes place when the current approaches the initial neutral position. For smaller values of the flow Reynolds number and buoyancy number, an initial acceleration of the flow near the source takes place, which makes the maximum flow velocity being greater than the current velocity at the inlet. The flow is then decelerated as the interfacial velocity shear generated mixing and

519 entrainment taking place along the slope. For larger flow Reynolds number and
520 buoyancy number, however, the flow is more turbulent and the shear-generated mixing
521 and entrainment occurs immediately as the flow intrudes into the environment. This
522 makes the maximum flow velocity at the region near the source being smaller than the
523 current velocity at the inlet. The shear-generated Kelvin–Helmholtz billows are seen to
524 appear at the top of the trailing fluid. Mixing and entrainment taking place at the
525 interface along the slope causes the increase of the current thickness with the distance
526 from the source. The simulations show that the spatially averaged thickness of the
527 current increases with the increase of the flow buoyancy number. Good agreement
528 between the numerical simulations and available laboratory measurements indicates
529 that the model can be applied to accurately simulate the spreading and motion of the
530 gravity current in complex environments. Some deviation between the simulated and
531 measured velocity takes place near the neutral buoyancy level where flow fluctuation is
532 strong. This discrepancy may suggest that the current 2D model may not be able to
533 capture the flow details near the neutral level and 3D numerical model will be required
534 for accurate simulation of the flow in this region. Comparison of the simulated and
535 measured velocity at large times indicates that the numerical model may overestimate
536 the mixing of flow with ambient fluid at that stage.
537
538 The flow simulated in this study has relatively low Reynolds number. For gravity
539 currents with the higher flow Reynolds number, the lobes and clefts may occur in the
540 front of the flow (Simpson 1997) and the current 2D model may not be able to capture

541 the details of such flow structures. In this case, 3D numerical models will be required to
542 run in order to capture these unstable events.
543
544 Acknowledgements: The research reported in this paper is financially supported by UK
545 Engineering and Physical Sciences Research Council (EPSRC: EP/G066264/1). The
546 constructive and insightful comments and suggestions made by three anonymous
547 Reviewers and the Associate Editor have significantly improved the quality of the final
548 paper.
549
550 **Notation**
551 *The following symbols are used in this paper:*
552 B_0=buoyancy number of the inflow
553 D=vertical distance from the top of slope to the position where the density of ambient
554 fluid equals to the density of inflow
555 d=the thickness of gravity current along slope
556 d_0=initial thickness of the inflow at the inlet
557 $\vec{g}$ = vector of gravity acceleration
558 g'_0=the reduced gravity acceleration
559 K_{pq} = the momentum exchange coefficient between phases
560 k= turbulent kinetic energy
561 k_{in} =turbulent kinetic energy at the inlet
562 N= buoyancy frequency of ambient fluid

563 P=pressure shared by phases

564 Q_0=initial volumetric flux per unit slot width

565 Re=the Reynolds number

566 Ri_g = the local gradient Richardson number across the interface

567 s= slope distance from the top of slope

568 s*=dimensionless slope distance from the top of slope

569 t=time

570 u_0=initial flow velocity along the x direction at the inlet

571 u_s=velocity component along the slope

572 u_{sm}=the maximum velocity along the slope

573 $\vec{v}$ =velocity vector

574 w=velocity in z- direction

575 x=horizontal coordinate

576 Z_0=water depth in the tank

577 z=vertical coordinate

578 α_q =volume fraction of phase q

579 θ=slope angle

580 μ= =dynamic viscosity of water

581 μ_t= turbulent (or eddy) viscosity

582 ν=kinetic viscosity of water

583 ρ_1= water density at the free surface

584 ρ_2=water density at the bottom of the tank

585 ρ_{in} = the initial density of inflow fluid

586 ρ_q = density of phase q

587 ρ_{top} = density of ambient fluid at the top of slope

588 $\overline{\rho}$ =mean density of the ρ_{top} and ρ_{in}

589 σ_k =turbulent Prandtl number for k

590 σ_ω=turbulent Prandtl number for ω

591 $\bar{\bar{\tau}}_q$ =stress-strain tensor of phase q

592 ε =dissipation rate of the turbulent kinetic energy

593 ω= the specific dissipation rate

594 ω_{in} = specific dissipation rate of at the inlet

595

596 **References**

597 Armi, L. (1986). "The hydraulics of two flowing layers with different densities." *J.*
598 *Fluid Mech.*, 163, 27-58.

599 Baines, P.G. (2001). "Mixing in flows down gentle slopes into stratified
600 environments." *J. Fluid Mech.*443, 237-270.

601 Baines, P.G. (2005). "Mixing regimes for the flow of dense fluid down slopes into
602 stratified environments." *J. Fluid Mech.*,538, 245-267.

603 Birman, V.K., Battandier, B.A., Meiburg, E. and Linden, P.F. (2007). "Lock exchange
604 flows in sloping channels." *J. Fluid Mech.*, 577, 53-77.

605 Birman, V.K., Meiburg, E. and Ungarish, M. (2007). "On gravity currents in stratified
606 ambient." *Phy. Fluids.* 19, 086602.

607 Bournet, P.E., Dartus, D., Tassin, B., and Vincon-Leite, B. (1999). "Numerical
608 investigation of plunging gravity current."*ASCE J. Hydraul. Eng.*,125(6), 584-594.
609 Britter, R.E., and Linden, P.F. (1980). "The motion of the front of a gravity current
610 travelling down an incline." *J. Fluid Mech.*, 99, 532-543.
611 Choi, S-U., and Garcia, M.H. (2002). "$k-\varepsilon$ turbulence modeling of gravity currents
612 developing two dimensionally on slope." *ASCE J. Hydraul.Eng.*, 128(1), 55-63.
613 Cokljat, D., Slack, M., Vasquez, S.A., Bakker, A., and Montante, G. (2006).
614 "Reynolds-Stress Model for Eulerian multiphase." *Prog. Comput. Fluid. Dyn*.,
615 6(1-3), 168-178.
616 Cuthbertson, A.J.S., Davies, P.A., Coates, M.J. and Guo, Y.K., (2004). "A Modelling study
617 of transient, buoyancy-driven exchange flow over a descending barrier." *Environ.*
618 *Fluid Mech.*, 4(2), 127-155.
619 Cuthbertson, A.J.S., Davies, P.A. and Guo, Y.K. (2006). "A model study of the
620 influence of submerged tidal barriers on estuarine mixing and exchange
621 processes." *ASCE J. Hydraul. Eng.*, 132 (10), 1033-1044.
622 Dai, A., Ozdemir, C.E., Cantero, M.I., and Balachanda, S. (2012). "Gravity currents
623 from instantaneous sources down a slope."*ASCE J. Hydraul.Eng.*,138(3), 237-246.
624 Dai, A. (2013). "Gravity Currents Propagating on Sloping Boundaries." *ASCE J.*
625 *Hydraul.Eng.*, 139(6), 593-601.
626 Dai, A. (2013). "Experiments on gravity currents propagating on different bottom
627 slopes." *J. Fluid Mech*., 731, 117-141.

628 Davies, P.A., Guo, Y.K., Boyer, D.L. and Folkard, A.M. (1995). "The flow generated by
629 the rotation of a horizontal disk in a stratified fluid." ***Fluid Dynamics Research***,
630 17, 27-47
631 Ellison, T.H. and Turner, J.S. (1959). "Turbulent entrainment in stratified flows." *J.*
632 *Fluid Mech*., 6, 423-448.
633 Falconer, R.A. (1992). "Flow and water quality modelling in coastal and inland water".
634 *J. Hydraul. Res*., 30, 437-452.
635 Ferziger, J.H. and Perić, M. (2002). *Computational methods for fluid dynamics*. 3rd
636 edition, Springer, Berlin.
637 Firoozabadi, B., Afshin, H., and Aram, E. (2009). "Three-dimensional modeling of
638 gravity current in a straight channel." *ASCE J. Hydraul. Eng.*,135(5), 393-402.
639 Guo, Y.K. (2014). "Numerical simulation of the spreading of aerated and nonaerated
640 turbulent water jet in a tank with finite water depth." *Journal of Hydraulic*
641 *Engineering*, 140(8). 10.1061/(ASCE)HY.1943-7900.0000903
642 Guo, Y.K., Davies, P.A., Cavalletti, A and Jacobs, P.T.G.A., (2000). "Topographic and
643 stratification effects on shelf edge flows." *Dynamics of Atmospheres and Oceans*,
644 31: 73-116.
645 Guo, Y.K., Wang, P. and Zhou, H. (2007). "Modelling study of the flow past
646 irregularities in a pressure conduit." *ASCE J. Hydraul. Eng.*, 133(6), 698-702.
647 Guo, Y.K., Zhang, L.X., Shen, Y.M. and Zhang, J.S., 2008. Modelling study of free
648 overfall in a rectangle channel with strip roughness, *ASCE J. Hydraul. Eng.*,
649 134(5), 664-668.

650 Guo, Y.K., Wu, X.G., Pan, C.H. and Zhang, J.S. (2012). "Numerical simulation of the
651 tidal flow and suspended sediment transport in the Qiantang Estuary." *ASCE J.*
652 *Waterway, Port, Coastal and Ocean Eng.*, 138(3), 192-203.
653 Härtel, C., Meiburg, E. and Necker, F., (2000) "Analysis and direct numerical
654 simulation of the flow at a gravity-current head. Part 1. flow topology and front
655 speed for slip and no-slip boundaries." *J. Fluid Mech.*, 418:189-212.
656 Holyer, J.Y., and Huppert, H.E., (1980). "Gravity current entering a 2-layer fluid." *J.*
657 *Fluid Mech.*, 100, 739
658 Jing, H., Guo, Y.K., Li, C. and Zhang, J. (2009). "Three dimensional numerical
659 simulation of compound meandering open channel flow by Reynolds stress
660 equation model." *International Journal for Numerical Methods in Fluids*,
661 59:927-943.
662 Launder, B.E., and Spalding, D.B. (1974). "The numerical computation of turbulent
663 flows." *Computer Methods in Applied Mechanics and Engineering*, 3,269–289.
664 Lawrence, G.A. (1993). "The hydraulics of steady two-layer flow over a fixed
665 obstacle." *J. Fluid Mech.*, 254, 605-633.
666 Mahdinia, M., Firoozabadi, B., Farshchi, M., Varnamkhasti, A., and Afshin, H. (2012).
667 "Large eddy simulation of lock-exchange flow in a curved channel." *ASCE J.*
668 *Hydraul. Eng.*, 138(1), 57–70.
669 Maxworthy, T., Leilich, J., Simpson, J.E. and Meiburg, E. (2002). "The propagation of
670 a gravity current into a linearly stratified fluid." *J. Fluid Mech.*, 453, 371-394.

671 Maxworthy, T., 2010. Experiments on gravity currents propagating down slopes. Part 2.
672 The evolution of a fixed volume of fluid released from closed locks into a long,
673 open channel. *J. Fluid Mech.*, 647, 2751.
674 Maxworthy, T., Nokes, R.I., 2007. Experiments on gravity currents propagating down
675 slopes. Part 1. The release of a fixed volume of heavy fluid from an enclosed lock
676 into an open channel. *J. Fluid Mech.*, 584, 433453.
677 Meiburg, E. and Kneller, B. (2010). "Turbidity currents and their deposits." *Annual*
678 *Review of Fluid Mech.*, 42, 135-156.
679 Mitsudera, H. and Baines, P. G. (1992). Downslope gravity currents in a continuously
680 stratified environment: a model of the Bass Strait outflow. *Proc., 11th*
681 *Australasian Fluid Mechanics Conference*, Hobart, Australia, 1017–1020.
682 Monaghan, J. J., Cas, R. A. F., Kos, A. M. Hallworth, M. (1999). "Gravity currents
683 descending a ramp in a stratified tank." *J. Fluid Mech.* 379, 39-70.
684 Moore, M. J. and Long, R. R. (1971). "An experimental investigation of turbulent
685 stratified shearing flow". *J. Fluid Mech.*, 49, 635-655.
686 Munroe, J.R., Voegeli, C., Sutherland, B.R., Birman, V. and Meiburg, E.H. (2009).
687 "Intrusive gravity currents from finite-length locks in a uniformly stratified fluid." *J.*
688 *Fluid Mech.*, 635, 245-273.
689 Ooi, S.K., Constantinescu, G. and Weber, L. (2007). "2D Large-eddy simulation of
690 lock-exchange gravity current flows at high Grashof numbers." *ASCE J. Hydraul.*
691 *Eng.*, 133(9), 1037–1047.

692 Özgökmen, T.M., Fischer, P.F. and Johns, W.E. (2006). "Product water mass formation
693 by turbulent gravity currents from a high-order nonhydrostatic spectral element
694 model." *Ocean Model.*,12, 237-267.
695 Rodi, W. (1993). *Turbulence models and their application in hydraulics: a*
696 *state-of-the-art review*. IAHR Monograph, 3rd edition, A.A. Balkema.
697 Spalding, D.B. (1980). *Mathematical modelling of fluid mechanics, heat-transfer and*
698 *chemical-reaction processes. A Lecture Course*, Imperial College, London.
699 Simpson, J.E., (1997). *Gravity currents in the environment and the laboratory*. 2nd
700 edition, Cambridge University Press.
701 Simpson, J.E., (1982). "Gravity currents in the laboratory, atmosphere, and ocean."
702 *Annual Review of Fluid Mech.*, 14, 213-234.
703 Ungarish, M. and Huppert, H.E. (2002). "On gravity currents propagating at the base of
704 a stratified ambient." *J. Fluid Mech.*, 458, 283-301.
705 Vasquez,S.A., and Ivanov,V.A.,(2000), "A Phase Coupled Method for Solving
706 Multiphase Problems on Unstructured Meshes." *Proc. ASME FEDSM'00:*
707 *ASME 2000 Fluids Engineering Division Summer Meeting*, ASMS, Boston.
708 pp743-748.
709 Versteeg,H.K., Malalasekera,W. (1995). *An Introduction to Computational Fluid*
710 *Dynamics: The Finite Volume Method.* 1st edition, Pearson Education Limited,
711 Essex, UK.
712 Wilcox, D.C. (2006). *Turbulence modeling for CFD.* 3rd edition, DCW Industries, Inc.
713 La Canada CA.

714 Wilcox, D.C. (2008). “Formulation of the k-omega Turbulence Model Revisited," ***AIAA***
715 ***Journal***, 46(11), 2823-2838.
716 Zhang, J.S., Guo, Y.K., Shen, Y.M., and Zhang, L.X. (2008). “Numerical Simulation of
717 Flushing of Trapped Salt Water from a Bar-Blocked Estuary.” *ASCE J. Hydraul.*
718 *Eng.*, 134(11), 1671–1676.
719 Zhu, D.Z. and Lawrence, G.A. (1998). “Non-hydrostatic effects in layered shallow
720 water flows.” *J. Fluid Mech.*, 355, 1-16.
721 Zhu, D.Z. and Lawrence, G.A. (2000). “Hydraulics of exchange flows.” *ASCE J.*
722 *Hydraul. Eng.*,126(12), 921-928.
723

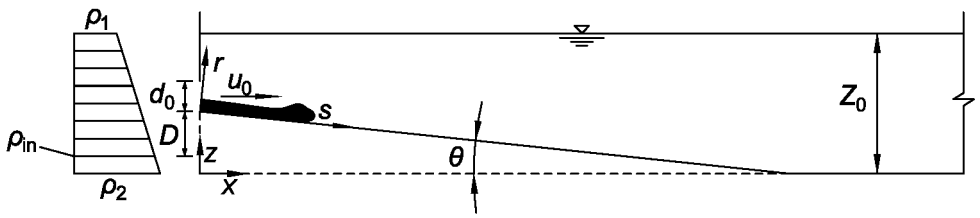

Figure 1. Sketch of the physical system under investigation

724

725

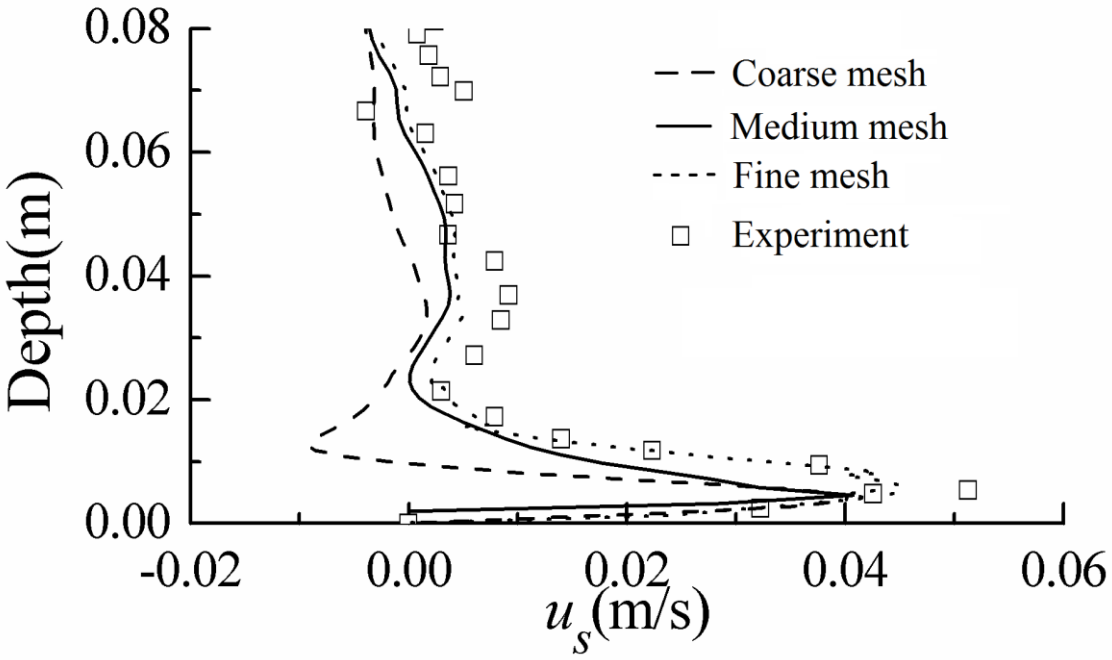

Figure 2. Mesh sensitivity study: effect of mesh size on the computational accuracy for gravity current descending a slope into a linearly stratified ambient, B_0=0.022 and *Re*=290

726

727

728

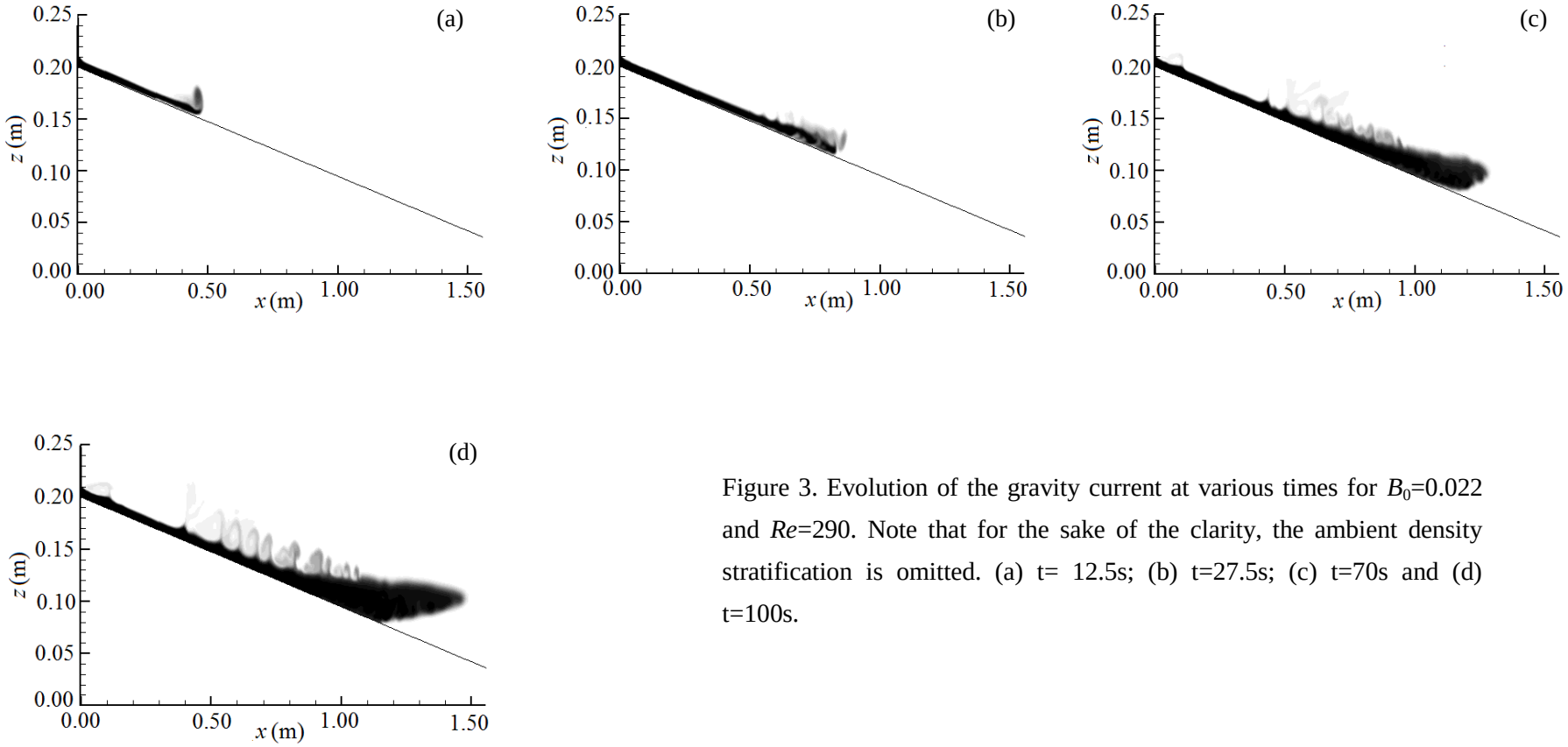

Figure 3. Evolution of the gravity current at various times for B_0=0.022 and *Re*=290. Note that for the sake of the clarity, the ambient density stratification is omitted. (a) t= 12.5s; (b) t=27.5s; (c) t=70s and (d) t=100s.

729
730
731

732

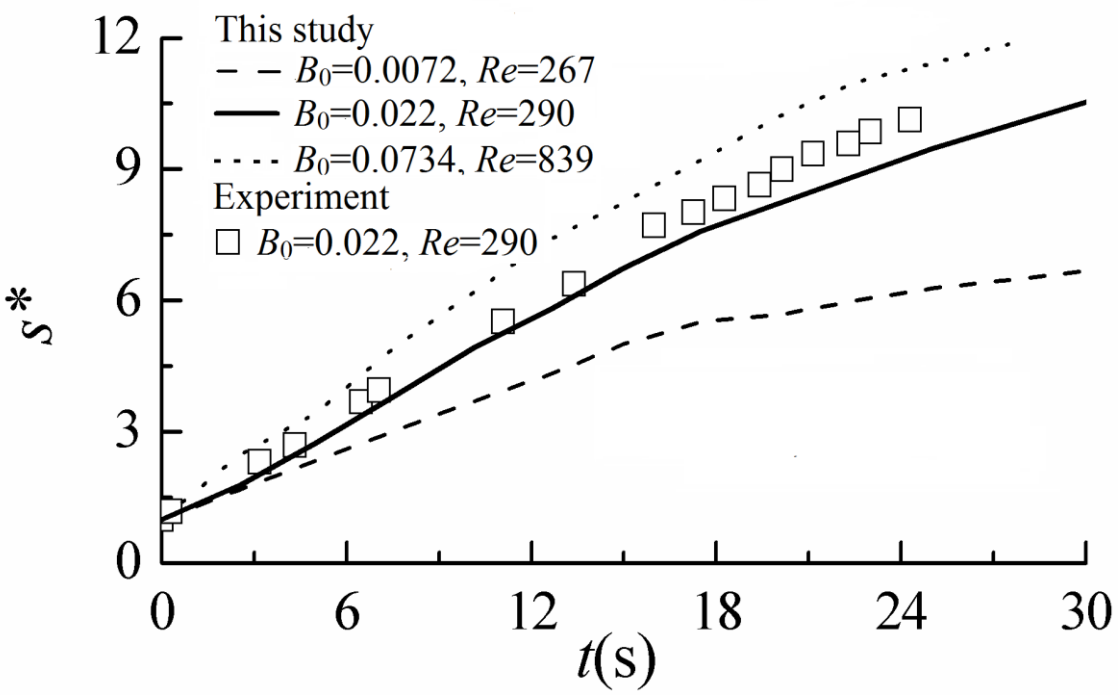

Figure 4. Dimensionless position of the current head versus time. Note that the time starts when the current reaches one D distance along the slope.

733

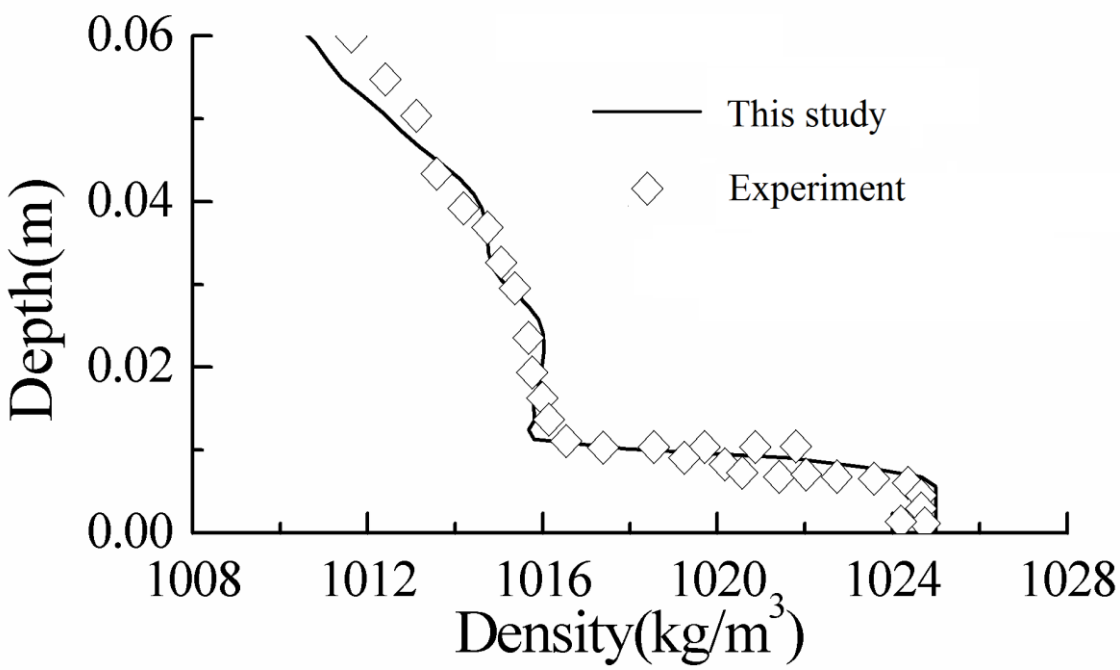

Figure 5. Vertical density profile at s=0.7 m for B_0=0.022 and Re=290.

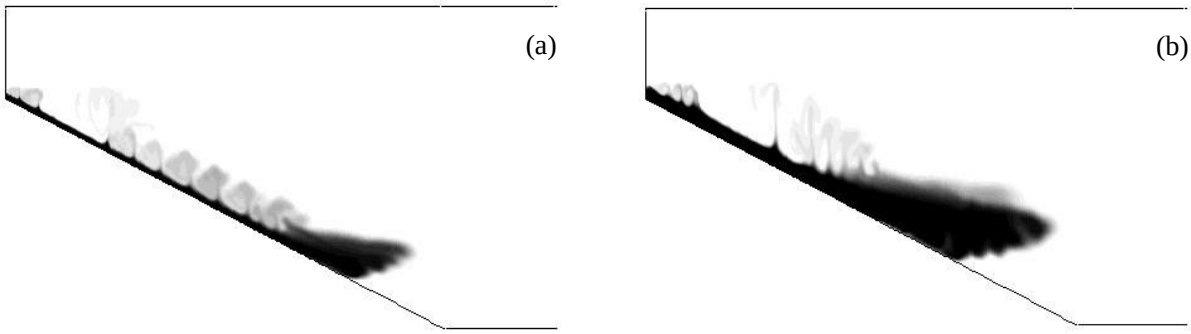

Figure 6. Typical shapes of gravity current near the inlet. Note that the vertical scale is five times of the horizontal scale. (a) B_0=0.0072, *Re*=267; (b) B_0=0.0462， *Re*=1121

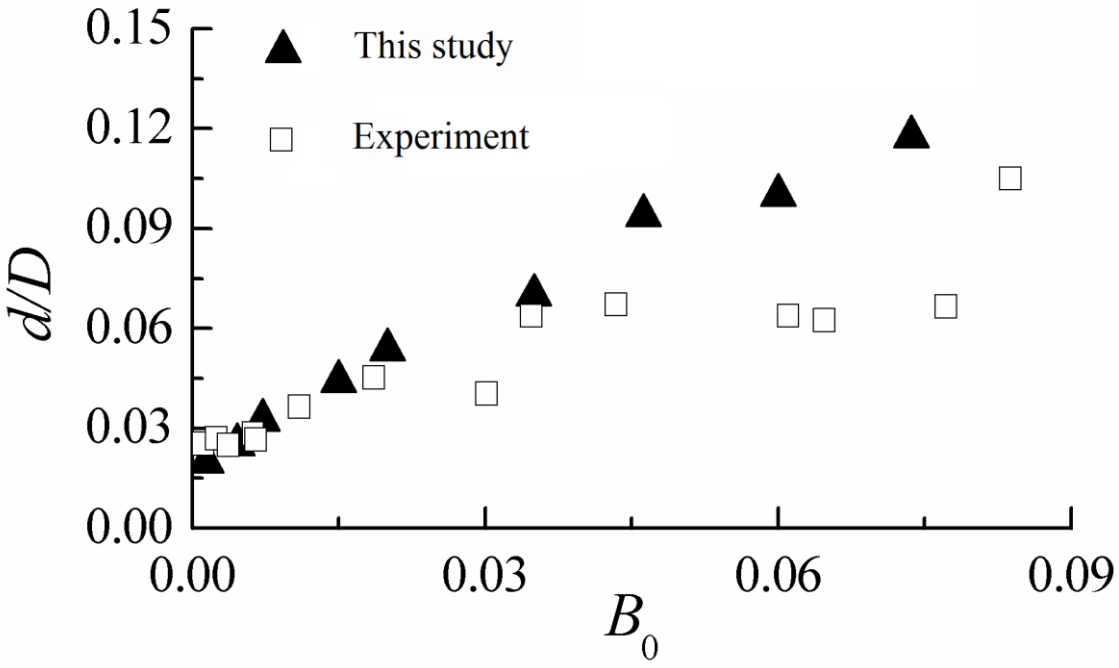

Figure 7. Comparison of the simulated and measured spatially averaged thickness of the gravity current versus B_0.

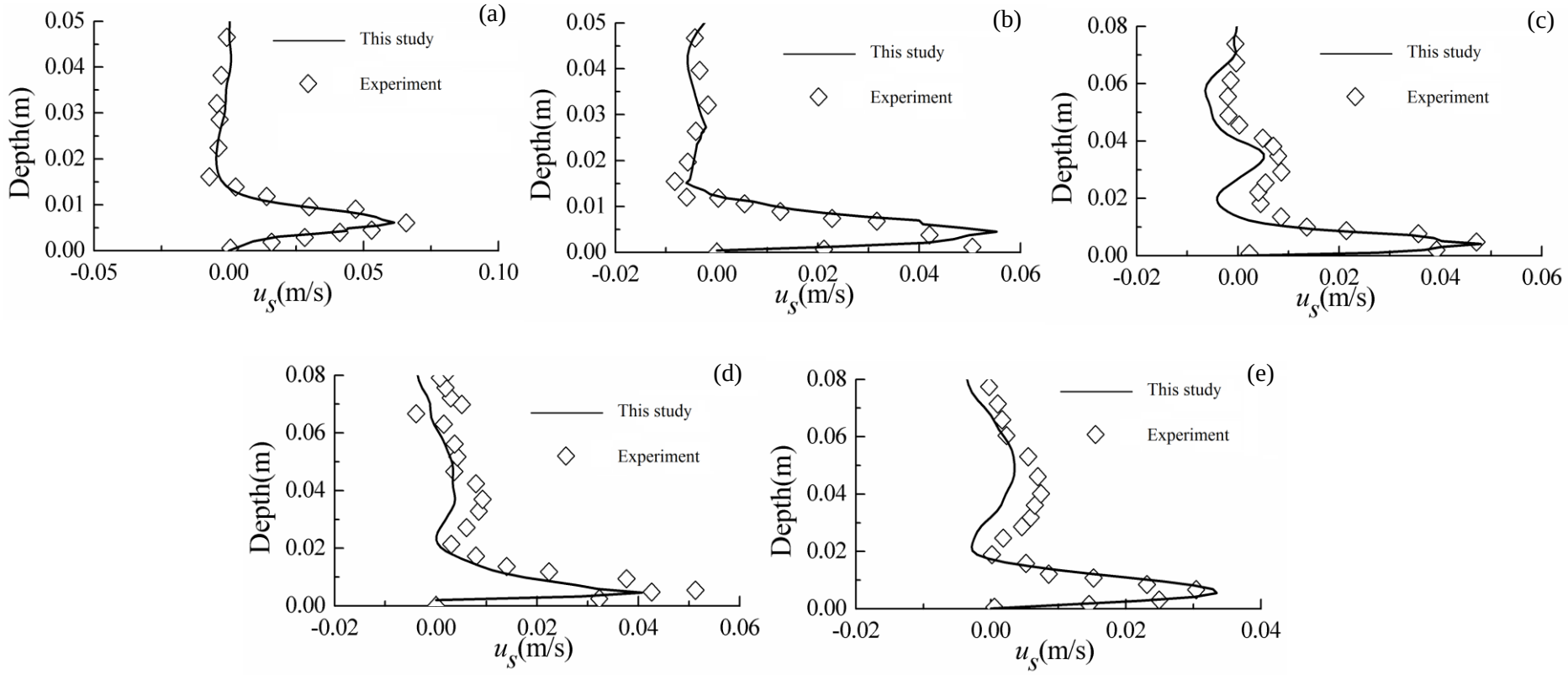

Figure 8. Comparisons of the simulated and measured (Mitsudera and Baines 1992) velocity profiles at different positions with B_0=0.022, *Re*=290. (a) s=0.1m; (b) s=0.3m; (c) s=0.5m; (d) s=0.7m; (e) s=0.9m.

764

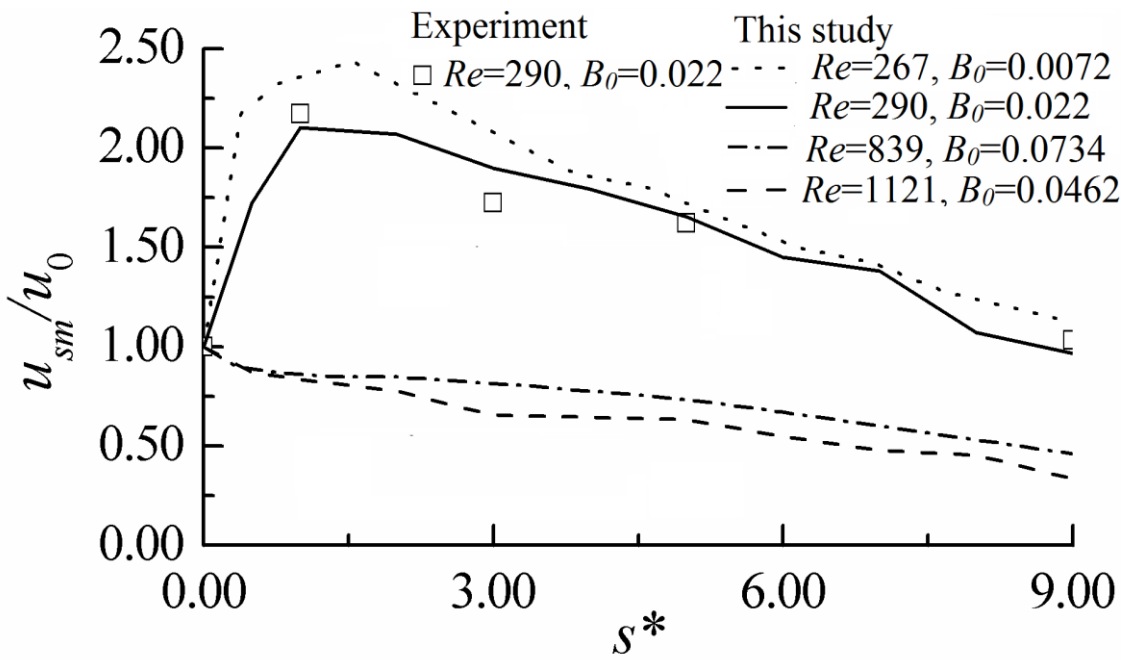

Figure 9. Comparison of the simulated and measured relative maximum velocity along the distance from the top of slope.

765